Research Article

Journal of Environmental Nanotechnology

Green-synthesized ZnO-functionalized *Passiflora foetida* Fiber/Epoxy Biocomposites: Mechanical, Thermostructural and Antibacterial Performance

E. Sathish[1*], J. Jeya Jeevahan[2], J. Dinakaran[3] and R. Ashok Raj[4]

[1]Department of Mechanical Engineering, Sathyabama Institute of Science and Technology, Chennai, TN, India
[2]Department of Mechanical Engineering, Godavari Global University, Rajahmundry, AP, India
[3]Department of Mechanical Engineering, Sri Muthukumaran Institute of Technology. Chikkarayapuram, Chennai, TN, India
[4]Department of Mechanical Engineering, J. J. College of Engineering and Technology, Tiruchirappalli, TN, India
Received: 25.07.2026 Accepted: 23.08.2026 Published: 30.09.2026
*sathishezhil1001@gmail.com

ABSTRACT

This study investigates the preparation and characterization of environmentally sustainable epoxy composites reinforced with *Passiflora foetida* fibers and ZnO nanoparticles green-synthesized using guava (*Psidium guajava*) leaf extract. The combined incorporation of *Passiflora foetida* fiber and guava-leaf-mediated ZnO nanoparticles into an epoxy matrix has been scarcely investigated, particularly for simultaneously improving its mechanical, thermal, dimensional, and antibacterial properties. Composite laminates were fabricated with fiber volume fractions of 10, 20, 30, and 40 vol.% and ZnO nanoparticle contents of 0, 1, 2, and 3 vol.% using the hand lay-up process. The fabricated composites were evaluated for their tensile, flexural, absorbed impact energy, hardness, physical, structural, thermal, and antibacterial properties. The composite containing 30 vol.% *Passiflora foetida* fiber and 2 vol.% ZnO nanoparticles exhibited the optimum mechanical performance, achieving a tensile strength, flexural strength, absorbed Izod impact energy, and hardness of 41.25 MPa, 75.4 MPa, 2.78 J, and 94.3 Shore D, respectively. FTIR, XRD, SEM, and TGA results provided supporting evidence of favorable fiber–matrix interactions, increased crystalline ordering, comparatively uniform nanoparticle distribution, and improved thermal stability in the optimized composite. The onset of major thermal degradation occurred at approximately 300 °C. The antibacterial activity of the optimized composite was evaluated against *Staphylococcus aureus* (*S. aureus*), *Bacillus subtilis* (*B. subtilis*), *Escherichia coli* (*E. coli*), and *Pseudomonas aeruginosa* (*P. aeruginosa*) using the agar disc-diffusion method. The composite exhibited inhibition zones of 22.8 ± 0.7, 20.9 ± 0.6, 18.6 ± 0.5, and 16.9 ± 0.5 mm, respectively, indicating antibacterial activity primarily associated with the contribution of the green-synthesized ZnO nanoparticles. Overall, the optimized composite demonstrated a favorable balance of mechanical performance, thermal resistance, dimensional stability, and antibacterial activity. These findings indicate its potential for interior components, furniture, packaging, and hygienic material applications, subject to further application-specific validation.

Keywords: *Passiflora foetida* fibre; ZnO nanoparticle; Antibacterial activity; Mechanical properties; Guava leaf extract.

1. INTRODUCTION

Growing environmental awareness and the increasing demand for sustainable engineering materials have accelerated the development of natural composites. In the present study, the developed material is specifically classified as a natural-fiber-reinforced epoxy/ZnO nanocomposite, comprising *P. foetida* fiber as the lignocellulosic reinforcement, epoxy as the polymer matrix, and green-synthesized ZnO nanoparticles as the nanofiller (Raja *et al.* 2026). Among the various reinforcement approaches, ceramic nanoparticles have demonstrated remarkable capability in enhancing the mechanical, thermal, and tribological characteristics of polymer composites (Subbarao *et al.* 2026). Zinc oxide (ZnO) nanoparticles have attracted particular attention owing to their excellent mechanical strength, high surface area, thermal stability, ultraviolet shielding capability, chemical stability, and intrinsic antibacterial activity. In the present epoxy system, hydroxylated ZnO surfaces and any residual oxygen-containing groups associated with green synthesis may promote polar and hydrogen-bonding interactions with cured epoxy functionalities and cellulose-rich fiber surfaces. When adequately dispersed, ZnO particles may also occupy interfacial microvoids, increase local mechanical interlocking, improve stress transfer, and hinder crack propagation. These mechanisms are treated as proposed interfacial explanations and are interpreted together with FTIR and SEM observations rather than as independently proven chemical bonding (Tasnim *et al.* 2024). Likewise, alkali-treated kenaf fiber-reinforced epoxy composites containing ZnO nanoparticles because of improved stress transfer and interfacial adhesion (Sathish *et al.* 2026).

Previous natural-fiber/ZnO composite studies consistently indicate that controlled nanoparticle addition

can improve stiffness, strength, wear resistance, thermal behavior, and interfacial characteristics. However, the reported benefits depend strongly on fiber chemistry, ZnO loading, nanoparticle dispersion, and matrix compatibility, while excessive nanoparticle aggregation can limit reinforcement efficiency (Yang *et al.* 2026). Moreover, most existing studies focus on conventional fibers such as jute, kenaf, flax, bamboo, and vetiver. Consequently, there remains a need to determine whether similar multifunctional improvements can be achieved using the less extensively investigated *P. foetida* fiber together with plant-mediated ZnO in epoxy (Demir, 2025). Similarly, flax/glass fiber-reinforced epoxy composites containing an optimum ZnO concentration exhibited superior tensile, flexural, and wear properties, while FESEM observations confirmed improved nanoparticle dispersion and fiber–matrix adhesion (Meravi and Panchore, 2025). Enhanced tensile, flexural, impact, hardness, and water resistance properties were also achieved in vetiver root fiber-reinforced epoxy composites through optimized ZnO loading (Ganesh *et al.* 2026). Furthermore, ZnO nanofiller incorporation substantially improved the mechanical and thermal performance of Cordia dichotoma fiber-reinforced composites by strengthening the interfacial bonding among the reinforcement and matrix (Seenivasan *et al.* 2025).

The reinforcing capability of ZnO nanoparticles has been successfully extended to various environmentally sustainable composite systems. Hybrid polyester composites reinforced with leather, cow hair, and chicken feather fibers exhibited the highest tensile and flexural properties when ZnO nanoparticles were employed as fillers, while SEM and FTIR analyses confirmed improved interfacial compatibility (Ali *et al.* 2024). A bio-inspired PDMS/SiO_2/ZnO hybrid interface further enhanced the tensile, flexural, thermal, antibacterial, and water-resistant properties of bamboo fiber-reinforced PLA composites by strengthening fiber–matrix compatibility (Fang *et al.* 2026).

Beyond mechanical enhancement, ZnO nanoparticles provide multifunctional characteristics that expand the application potential of polymer composites. The incorporation of AgO/ZnO nanostructures improved mechanical strength, thermal stability, antibacterial activity, biodegradability, and moisture resistance in sustainable packaging films (Koshy and Sangeetha, 2026). Similarly, cassava starch/chitosan bioplastics reinforced with pineapple leaf fibers and ZnO nanoparticles exhibited enhanced mechanical strength, prolonged antibacterial activity, and accelerated biodegradation suitable for eco-friendly food packaging (Armynah *et al.* 2022). ZnO-coated soybean hull fibers also demonstrated improved surface characteristics, thermal stability, and resistance to bacterial adhesion, highlighting their potential for functional textile applications (Sakti *et al.* 2025). Furthermore, ZnO and Al_2O_3 nanocoatings deposited on cotton and viscose fabrics produced strong antibacterial behaviour against *E. coli* and *S. aureus* while maintaining good biocompatibility (Popescu *et al.* 2019).

In plant-mediated ZnO synthesis, phytochemical-derived hydroxyl, carbonyl, phenolic, and related functional groups can participate in precursor conversion and remain associated with the nanoparticle surface. Such surface-associated organic functionalities may reduce uncontrolled aggregation, influence dispersion, and modify interfacial interactions when ZnO is incorporated into a polymer composite. These effects can differ from conventionally synthesized ZnO because plant-mediated particles may retain phytochemical-derived surface functionalities; however, improved composite adhesion must be verified experimentally rather than assumed (Abd *et al.* 2026). The phytochemical richness of *Passiflora foetida* was further demonstrated through ATR-FTIR metabolomic investigations, where ethanol leaf extracts prepared by sonication possessed the highest phenolic and flavonoid contents, while freeze-drying effectively preserved bioactive metabolites responsible for antioxidant activity (Ning *et al.* 2023). Likewise, ZnO treatment has also improved the mechanical performance of other natural-fiber/polymer systems, further supporting the use of ZnO as an interfacial and functional nanofiller (Tumusiime *et al.* 2023).

Although ZnO-modified jute, banana, kenaf, flax, vetiver, and *Cordia dichotoma* fiber composites have been investigated, these studies predominantly employ established reinforcement systems. In contrast, comparatively limited information is available on integrating *Passiflora foetida* fiber with plant-mediated ZnO nanoparticles in an epoxy matrix and evaluating the resulting mechanical, thermal, structural, and antibacterial properties within the same composite system. This gap provides the scientific basis for the present investigation. Previous studies have characterized *Passiflora foetida* as a lignocellulosic reinforcement and examined its potential for composite and paperboard applications; however, its use in green-ZnO-modified epoxy composites remains comparatively limited. Therefore, the novelty of the present work lies specifically in combining *P. foetida* fiber with guava-leaf-mediated ZnO nanoparticles and evaluating multifunctional composite performance. Moreover, limited studies have investigated the integration of green-synthesized guava leaf-derived ZnO nanoparticles with *Passiflora foetida* fiber to simultaneously improve the mechanical, thermal, and antibacterial behavior of composites. Existing studies primarily focus on conventional natural fibers and chemically synthesized nanoparticles, with limited emphasis on sustainable nanoparticle synthesis and multifunctional composite development. To address this gap, the present study develops a novel bio-composite reinforced with

Passiflora foetida fiber and green-synthesized guava leaf-derived ZnO nanoparticles. The effect of fiber and nanoparticle contents on the mechanical, structural (FTIR, XRD, and SEM), thermal (TGA), and antibacterial properties was systematically investigated. The optimized composite demonstrated superior multifunctional performance, providing an environmentally friendly and sustainable material.

2. MATERIALS AND METHODOLOGY

2.1 Materials

Passiflora foetida fibres and guava leaves were collected from the local region in Erode, Tamil Nadu. The polymer matrix consisted of LY556 epoxy resin and HY951 hardener. Following the manufacturer's specifications at a ratio of 10:1, the resin and hardener were blended. Both materials were obtained from Kovai Cheenu Enterprises, Coimbatore, India.

2.2 Preparation of *Passiflora foetida* Fiber

Passiflora foetida stems were immersed in tap water at a fiber-to-water ratio of 1:20 (w/v) and retted for 6 days at 27 ± 2 °C and an initial pH of 7.0 ± 0.2. The retting water was replaced every 24 h to limit microbial accumulation and maintain consistent conditions. After retting, the softened stems were manually decorticated to recover the fibers. The extracted fibers were cleaned and dried at 60 °C for 1 day. The dried fibers were immersed in 5 wt.% NaOH solution at a fiber-to-solution ratio of 1:20 (w/v) and treated at 27 ± 2 °C for 1 h under occasional stirring. Approximately 2 L of NaOH solution was used for every 100 g of dried fiber. After treatment, the fibers were repeatedly washed with deionized water until the final wash water reached pH 7.0 ± 0.2. The treated fibers were cut into 1 cm lengths and stored in sealed containers for subsequent composite fabrication. The 10 mm fibers were used as randomly oriented discontinuous reinforcement. Before lay-up, each calculated fiber quantity was divided into three equal portions, manually separated, and uniformly distributed over the mold using a marked grid to minimize fiber clustering and preferential orientation. Fig. 1 indicates the SEM image of raw and treated *Passiflora foetida* Fiber.

2.3 Green Synthesis of Guava Leaf-derived ZnO Nanoparticles

Fresh guava leaves were washed thoroughly with deionized water. Twenty grams of chopped leaves were heated in 200 mL of deionized water at 80 °C for 20 min. The extract was cooled to room temperature and filtered through Whatman No. 1 filter paper. Subsequently, 100 mL of leaf extract was mixed with 200 mL of 0.1 M $Zn(NO_3)_2 \cdot 6H_2O$ solution, corresponding to an extract-to-precursor volume ratio of 1:2 and a final reaction volume of 300 mL. The mixture was stirred magnetically at 600 rpm and 80 °C for 2 h. The pH was adjusted to 10.0 ± 0.1 by adding 1 wt.% NaOH dropwise while continuously monitoring with a calibrated pH meter. The resulting suspension was aged for 12 h at room temperature and centrifuged at 8000 rpm for 15 min. The precipitate was washed three times with deionized water and twice with ethanol, dried at 80 °C for 12 h, and calcined at 450 °C for 3 h using a heating rate of 5 °C min^{-1}. Similarly, the study employed a green synthesis method for the preparation of ZnO nanoparticles.

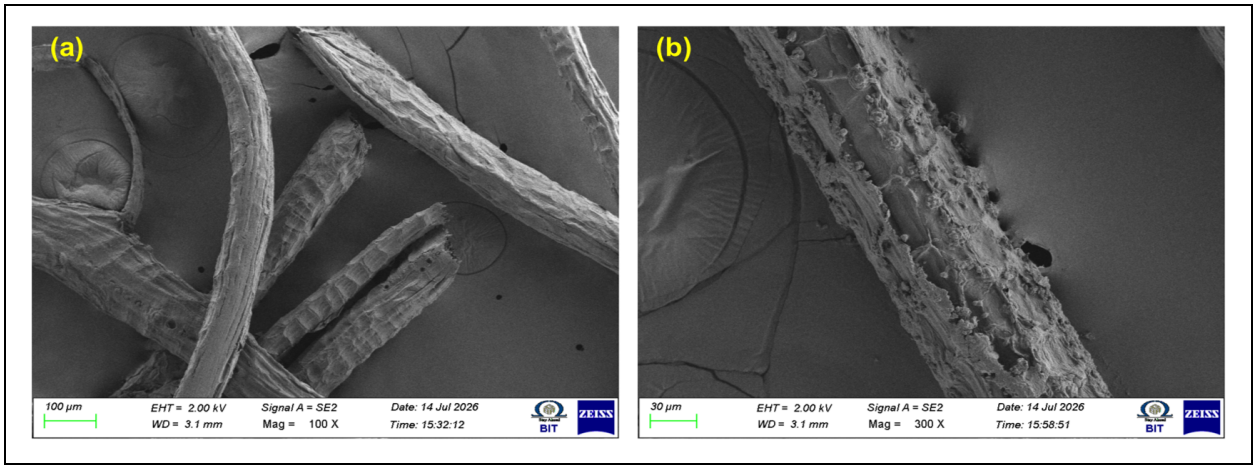

Fig. 1: Scanning electron microscope image of (a) raw and (b) treated *Passiflora foetida* Fiber

2.4 Fabrication of Composite

The composite laminates were produced using the traditional hand lay-up technique (Gupta *et al.* 2026). A mold measuring 300 mm × 300 mm × 3 mm was prepared by applying wax and covering the mold to facilitate easy demolding. The epoxy matrix was prepared by mixing the resin and hardener and was

initially spread over the mold surface. The required ZnO nanoparticles were initially dispersed in the epoxy resin by mechanical stirring at 500 rpm for 30 min, followed by ultrasonication for 20 min. The mixture was vacuum-degassed at −0.08 MPa for 10 min before adding HY951 hardener at a resin-to-hardener ratio of 10:1. The chopped fibers were divided into three equal portions and distributed as three random reinforcement layers. Each layer was impregnated with the ZnO–epoxy mixture and consolidated using a hand roller to remove entrapped air and maintain uniform thickness. Subsequently, *Passiflora foetida* fibers and green-synthesized ZnO nanoparticles were incorporated according to the specified volume fractions (Table 1) and uniformly distributed by hand lay-up.

Table 1. Composite formulation based on the volume fractions of *Passiflora foetida* fiber, epoxy resin and ZnO nanofiller

S. No.	Sample Code	*Passiflora foetida* Fibre (Vol %)	ZnO Nanofiller (Vol %)	Epoxy Resin (Vol %)
1	S1	10	1	89
2	S2	20	1	79
3	S3	30	1	69
4	S4	40	1	59
5	S5	10	2	88
6	S6	20	2	78
7	S7	30	2	68
8	S8	40	2	58
9	S9	10	3	87
10	S10	20	3	77
11	S11	30	3	67
12	S12	40	3	57
13	S13	10	0	90
14	S14	20	0	80
15	S15	30	0	70
16	S16	40	0	60

Constituent masses were calculated from their target volume fractions using $m_i = V_i \rho_i$, where m_i, V_i, and ρ_i represent the mass, volume, and density of constituent i, respectively. Densities of $1.38\ \mathrm{g\ cm^{-3}}$ for *Passiflora foetida* fiber, $5.61\ \mathrm{g\ cm^{-3}}$ for ZnO, and $1.17\ \mathrm{g\ cm^{-3}}$ for the cured epoxy system were used. The constituent mass was calculated as:

$$m_i = \frac{V_{f,i}}{100} \times V_c \times \rho_i$$

where $V_{f,i}$ is the target volume percentage and V_c is the total laminate volume of $270\ \mathrm{cm^3}$.

A hand roller was employed to eliminate air bubbles and improve uniform dispersion of the epoxy matrix throughout the reinforcement. The lay-up arrangement was repeated till the required composite thickness was attained. The laminates were cured in the closed mold at 27 ± 2 °C for 24 h under a uniformly distributed pressure of 0.02 MPa. After demolding, they were post-cured in a hot-air oven at 60 °C for 2 h and conditioned at 27 ± 2 °C and 50 ± 5% relative humidity for 48 h before testing. The overall fabrication procedure of the composites is shown in Fig. 2.

2.5 Testing of mechanical properties

Mechanical specimens were cut from the laminates and conditioned at 23 ± 2 °C and 50 ± 5% relative humidity for 48 h. Tensile testing was conducted according to ASTM D3039 using specimens measuring 250 × 25 × 3 mm, a gauge length of 150 mm, and a crosshead speed of 1.5 mm $\mathrm{min^{-1}}$. Flexural testing was conducted according to ASTM D790 using specimens measuring 127 × 12.7 × 3 mm in a three-point configuration at 2 mm $\mathrm{min^{-1}}$. A support span of 48 mm was used, corresponding to a span-to-depth ratio of 16:1 for the 3 mm-thick specimens. Loading was applied centrally using a three-point bending fixture. Notched Izod impact tests were performed according to ASTM D256 (Edlabadkar *et al.* 2026) using specimens measuring 63.5 × 12.7 × 3 mm. A 45° V-notch with a depth of 2.54 mm and a tip radius of 0.25 mm was machined at the specimen midpoint, while Shore D hardness was measured according to ASTM D2240 (Harish *et al.* 2026). Five specimens from each composition were tested, and the results were reported as mean ± standard deviation.

2.6 Characterization

The structural, chemical, and morphological behavior of the fabricated samples were analyzed using X-ray diffraction (XRD), Fourier transform infrared (FTIR), and scanning electron microscopy (SEM) analyses. FTIR spectroscopy was employed to recognize the functional groups in the composites in the range of 4000–400 $\mathrm{cm^{-1}}$. Crystallinity and phase identification were carried out using a Rigaku Miniflex 600 X-ray Diffractometer with Cu-Kα radiation (λ = 1.5406 Å), operating at 40 kV and 15 mA. Data were collected over a 2θ range of 10°–80° with a scan rate of 2°/min. SEM was performed on raw fibers, alkali-treated fibers, synthesized ZnO nanoparticles, and tensile-fractured composite surfaces using a ZEISS Gemini SEM operated at 10 kV. Fiber and composite specimens were dried, mounted on aluminium stubs using conductive carbon tape, and sputter-coated with gold for 60 s. Images were acquired at representative magnifications ranging from

500× to 20,000×. ZnO particles were examined at 20,000×–50,000×, and particle diameters were measured from at least 100 particles. Magnification and calibrated scale bars were included in every micrograph. Samples were sputter-coated with a thin gold layer to prevent charging.

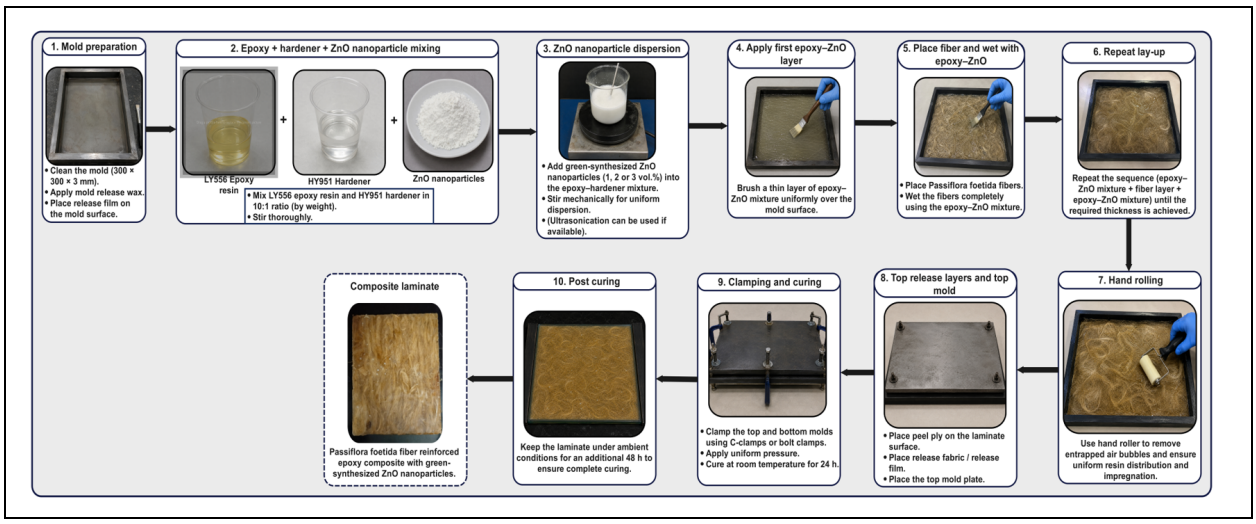

Fig. 2: A representation of the fabrication of the composite

2.7 Physical Properties

Density was determined using five rectangular specimens measuring 30 × 30 × 3 mm. Each specimen was dried at 60°C for 24 h, cooled in a desiccator, weighed to an accuracy of 0.001 g, and measured using a digital micrometer. Density was calculated as $\rho = m/(Lwt)$, where m is the dry mass and L, w, and t are the specimen length, width, and thickness, respectively. Water absorption was evaluated according to ASTM D570 using five specimens measuring 30 × 30 × 3 mm. The specimens were dried at 60 °C for 24 h, cooled in a desiccator, and weighed. They were immersed in deionized water at 23 ± 2 °C and removed after 2, 6, 12, and 24 h. Surface water was removed using absorbent paper, and the specimens were weighed within 1 min. Water absorption was calculated as $[(W_t - W_0)/W_0] \times 100$, where W_0 and W_t are the initial dry and immersed masses, respectively. Thickness swelling was measured using the same specimens and immersion conditions employed for water absorption. Thickness was measured at five marked locations before immersion and after 24 h using a digital micrometer with 0.01 mm resolution. Thickness swelling was calculated as $[\ (t_{24} - t_0)/t_0] \times 100$, where t_0 and t_{24} represent the mean specimen thickness before and after 24 h immersion, respectively. This procedure was adapted from ASTM D570 and is reported as a laboratory thickness-swelling measurement.

$$\text{Water absorption (\%)} = \frac{W_{\text{final}} - W_{initial}}{W_{initial}} \times 100 \quad \text{... (1)}$$

$$\text{Swelling Thickness} = \frac{t_{\text{final}} - t_{initial}}{t_{initial}} \times 100 \quad \text{... (2)}$$

2.8 Thermal Gravimetric Analysis (TGA)

Thermogravimetric analysis was performed using a TA Instruments Q50 thermogravimetric analyzer. Approximately 5 ± 0.5 mg of each sample was placed in an alumina pan and heated from 30 to 600 °C at 10 °C min^{-1} under nitrogen flowing at 50 mL min^{-1}. The onset degradation temperature was determined from the tangent-intersection method applied to the TGA curve, while maximum degradation temperatures were obtained from the corresponding DTG peaks.

2.9 Antibacterial Evaluation

Antibacterial activity was evaluated using Mueller–Hinton agar against *Bacillus subtilis* ATCC 6633, *Staphylococcus aureus* ATCC 25923, *Escherichia coli* ATCC 25922, and *Pseudomonas aeruginosa* ATCC 27853. Bacterial suspensions were adjusted to 0.5 McFarland, corresponding to approximately 1.5 × 10^8 CFU mL^{-1}. Composite discs measuring 10 mm in diameter were sterilized under UV light for 30 min on each side and placed on inoculated agar plates. The plates were incubated at 37 °C for 24 h. Inhibition zones were measured in two perpendicular directions using a digital caliper, and the mean diameter was calculated from five replicate plates.

Disc diffusion was selected as an initial screening method to determine whether antibacterial species associated with the ZnO-containing composite could inhibit bacterial growth at the composite–agar interface. Because nanoparticle and Zn^{2+} diffusion may be restricted by the cured epoxy matrix, inhibition-zone measurements were interpreted qualitatively and not as a direct measure of total bactericidal efficiency. Future

work will employ viable-cell reduction or direct-contact testing to quantify antibacterial activity.

3. RESULTS AND DISCUSSION

3.1 Mechanical Behavior of the Composites

The mechanical performance of the developed composites was assessed by TS, FS, IS, and Shore D hardness assessments to determine the influence of *Passiflora foetida* fiber and ZnO nanofiller contents. The TS of the fabricated *Passiflora foetida* fiber-reinforced epoxy composites exhibited a pronounced dependence on the fiber and ZnO nanofiller volume fractions. As illustrated in Fig. 3, the tensile strength ranged from 18.4 MPa to 41.25 MPa across the different composite formulations.

The tensile strength increased with increasing *Passiflora foetida* fiber content from 10 to 30 vol.% for all ZnO nanofiller loadings, followed by a noticeable decrease at 40 vol.%. The maximum tensile strength of 41.25 MPa was attained at 30% fiber and 2 % ZnO nanofiller (S7). The enhancement in TS up to 30 % is due to efficient load dispersion between the epoxy and the reinforcement. At 30 vol.%, the fibers were uniformly dispersed within the matrix, promoting effective stress distribution and delaying crack initiation. Furthermore, the incorporation of ZnO nanofillers improved the fiber–matrix interfacial bonding, thereby reducing void formation and enhancing the overall mechanical integrity of the composite.

A reduction in TS was noted when the fiber volume was raised to 40 vol.%. This deterioration is primarily associated with inadequate resin impregnation, fiber agglomeration, and increased fiber–fiber contact, which generate stress concentration sites and facilitate premature crack propagation. The influence of ZnO nanofiller content was also evident in the tensile behavior of the composites. Among the investigated formulations, the composites containing 2 vol.% ZnO nanofiller consistently exhibited higher tensile strength than those reinforced with 1 vol.% or 3 vol.% ZnO, as shown in Fig. 3. At 1 vol.%, the amount of nanofiller was insufficient to provide significant reinforcement or improve interfacial adhesion. In contrast, increasing the nanofiller loading to 3 vol.% promoted particle agglomeration, which disrupted the continuity of the epoxy matrix and reduced the efficiency of stress transfer. Therefore, a ZnO nanofiller content of 2 vol.% was identified as the optimum level, providing enhanced reinforcement while minimizing structural defects. Previous studies state that the addition of ZnO nanoparticles improved the tensile behavior of banyan fiber-reinforced epoxy composites, with the optimum tensile strength achieved at 4 wt.% ZnO, corresponding to a 58.97% improvement over the unfilled composite. The improved tensile behavior was due to the homogeneous dispersion of ZnO nanoparticles, which strengthened the reinforcement–matrix interfacial bonding and facilitated efficient stress transfer (Muniyasamy *et al.* 2025).

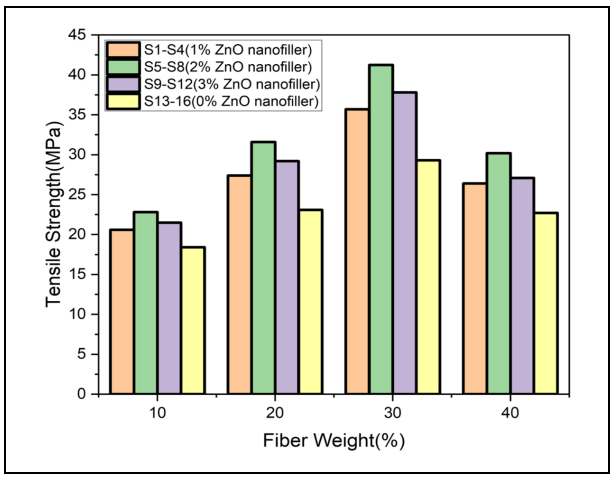

Fig. 3: Tensile strength of *Passiflora foetida* fiber- ZnO nanofiller composites

The flexural strength (FS) of the fabricated composites varied from 36.5 MPa to 75.4 MPa. As indicated in Fig. 4, the FS enhancement is till 30% *Passiflora foetida* fiber, then reduced at 40 vol.%. The highest flexural strength (75.4 MPa) was obtained for the S7 composite. The improvement in FS was due to efficient stress distribution between the epoxy and the fibers under bending loads. At 30 vol.% fiber content, the fibers and ZnO nanofillers were uniformly dispersed, resulting in enhanced interfacial bonding, increased stiffness, and improved resistance to bending deformation. In addition, the ZnO nanofillers enhanced the rigidity of the epoxy matrix, thereby minimizing localized deformation during flexural loading.

A decrease in flexural strength was observed at 40 vol.% fiber content due to insufficient matrix impregnation, non-uniform fiber distribution, and increased fiber–fiber interactions. These factors promoted the formation of microcracks and interfacial defects under bending stresses, leading to premature failure. Composites reinforced with 3 vol.% ZnO nanofiller exhibited lower flexural strength than those containing 2 vol.%, primarily because of nanoparticle agglomeration and the resulting interfacial discontinuities. In contrast, 1 vol.% ZnO provided only a moderate improvement owing to the limited reinforcing effect. These results demonstrate that 2 vol.% ZnO nanofiller provides the optimum reinforcement by preserving structural integration and improving homogeneous stress dispersion. These observations confirm that the addition of ZnO nanoparticles mainly improved the flexural behaviour of *Nelumbo nucifera* fiber-reinforced epoxy composites, increasing the flexural strength from 42 MPa to 60 MPa, representing a 30.48% enhancement. The improved bending behavior

was attributed to better interfacial adhesion and efficient stress transfer between the ZnO nanoparticles, natural fibers, and epoxy matrix (Senniangiri *et al.* 2025).

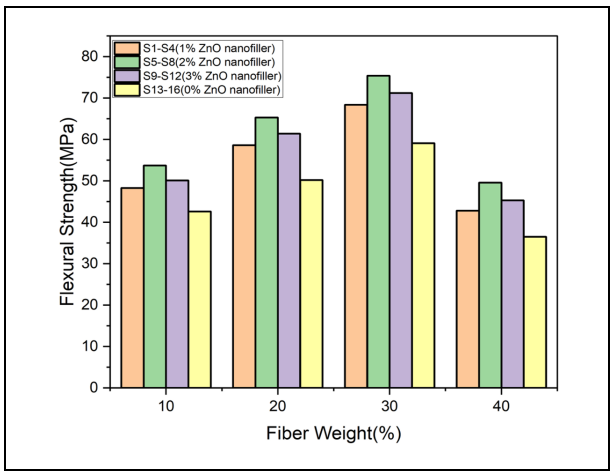

Fig. 4: Flexural strength of *Passiflora foetida* fiber- ZnO nanofiller composites

The impact strength (IS) of the composites illustrated in Fig. 5 ranges from 1.12 J to 2.78 J, indicating the relatively stiff behavior of epoxy composites. The S7 composite showed the maximum impact strength (IS), representing higher resistance to sudden loading. The improvement in impact performance with increasing fiber content up to 30 % is associated with improved energy dissipation through failure mechanisms like controlled interfacial debonding, matrix cracking, and fiber pull-out. The incorporation of ZnO nanofillers further strengthened the fiber–matrix interface, facilitating more effective distribution of impact energy throughout the composite. However, increasing the fiber content to 40 vol.% or the ZnO nanofiller loading to 3 vol.% resulted in reduced impact strength because of increased stiffness, lower matrix ductility, and nanoparticle agglomeration. These faults act as localized stress regions that promote crack nucleation and extension, thereby reducing the impact resistance of the composites. As reported in prior studies, the addition of ZnO nanoparticles improved the impact behavior of casuarina fiber-reinforced epoxy composites with the ZnO-filled composite achieving the maximum impact strength of 7.5 kJ/m². The improvement was attributed to enhanced fiber–matrix interfacial bonding and efficient energy absorption, resulting in superior resistance to crack initiation and propagation under impact loading (Barve *et al.* 2025). The results suggest that an optimum balance between fiber reinforcement and matrix toughness is essential for achieving improved impact resistance.

The hardness of the composites ranged between 77.2 and 94.3, as presented in Fig. 6. Hardness increased progressively up to 30% fiber content, then decreased slightly at 40%. The S7 shows the maximum hardness of 94.3 Shore D. The increase in hardness is due to the combined strengthening impact of *Passiflora foetida* fibers and ZnO nanofillers, which improved resistance and surface firmness to confined indentation. The ZnO nanofillers also contributed to matrix densification, thereby improving surface rigidity and wear resistance. In contrast, excessive nanofiller loading promoted particle agglomeration and weak interfacial regions, leading to a reduction in hardness. Composites without ZnO reinforcement consistently showed minimum hardness, demonstrating the advantageous role of ZnO nanofillers in enhancing the surface toughness of the developed epoxy composites. According to previous study, the incorporation of 1 wt.% ZnO nanoparticles significantly improved the hardness of woodnut fiber-strengthened polyester composites, achieving a maximum hardness of 455.5 HL at 15 wt.% fiber loading. The enhanced hardness improved filler dispersion and stronger fiber–matrix interfacial bonding, which increased the composite's resistance to surface deformation (Soshi *et al.* 2026).

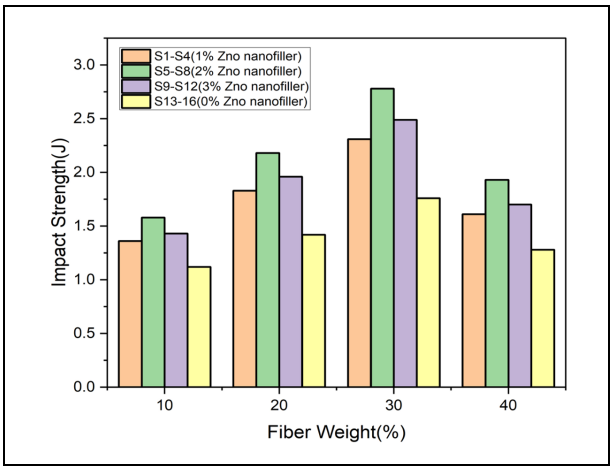

Fig. 5: Impact strength of *Passiflora foetida* fiber- ZnO nanofiller composites

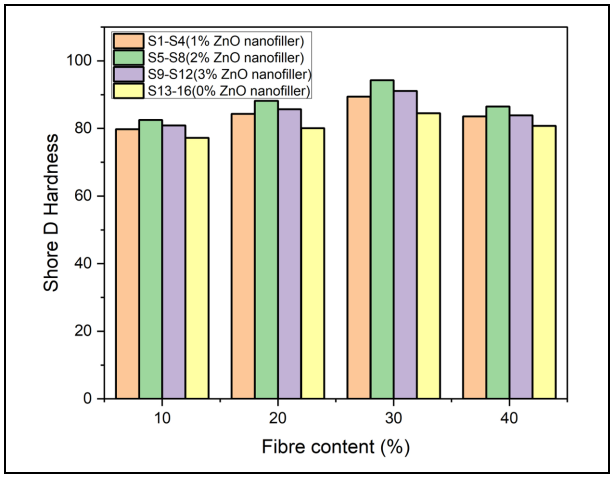

Fig. 6: Hardness of *Passiflora foetida* fiber- ZnO nanofiller composites

The fiber content of 30 vol.% was selected for structural analysis because it exhibited the optimum mechanical properties among all the fabricated composites. Maintaining a constant fiber content while varying the ZnO nanofiller concentration (0, 1, 2, and 3 vol.%) enabled the effect of the nanofiller on the chemical interactions and fiber–matrix interfacial bonding to be evaluated without the influence of fiber content variation.

3.2 Characterization of 30 vol.% Fiber Composites with Varying ZnO Nanofiller Content

XRD analysis was performed to investigate the phase composition of the fabricated sample and to find the effect of ZnO nanofiller incorporation on their structural characteristics. The diffracted peak exhibited the characteristics diffraction peak of cellulose I together with a broad amorphous range associated with the epoxy. Among the investigated formulations, the 2 vol.% ZnO nanofiller (S7) composite shows the maximum CI, denotes a greater proportion of ordered cellulose domains. The increase in crystallinity is associated with improved toughness and Stress-bearing capacity, it agrees well with the higher mechanical properties.

The S3 composite exhibited a relatively broad diffraction peak at approximately 2θ = 22.44°, corresponding to the (002) plane of cellulose I with a crystallinity index of approximately 54%, indicating moderate crystalline order and comparatively lower mechanical strength (Fig. 7). In contrast, the S7 composite showed a sharp and more intended diffraction peaks at 2θ ≈ 22.4°, accompanied by a reduced amorphous background and the highest crystallinity index of approximately 72%. This increase in crystallinity reflects a more ordered cellulose structure, contributing to enhanced stiffness and mechanical strength. The S11 composite exhibited a broader diffraction peak with a crystallinity index of approximately 66%, suggesting that excessive ZnO nanofiller promoted particle agglomeration and hindered the formation of a well-organized crystalline structure, thereby reducing the reinforcing efficiency. The raw fiber composite (D30) displayed the broadest diffraction peak and the lowest crystallinity index (approximately 46%), which can be attributed to the presence of residual hemicellulose and lignin within the untreated fiber structure. Overall, the XRD results demonstrate that an optimum ZnO nanofiller loading of 2 vol.% enhances the crystalline characteristics of the cellulose phase, thereby contributing to the enhanced stiffness and mechanical behavior of the composites. Earlier research reported that the XRD analysis confirmed the successful formation of crystalline ZnO nanoparticles with a characteristic hexagonal wurtzite crystal structure synthesized using *Passiflora foetida* leaf extract. The well-defined diffraction peaks indicated high crystallinity and phase purity, demonstrating the effective green synthesis of ZnO nanoparticles (Loganathan *et al.* 2025).

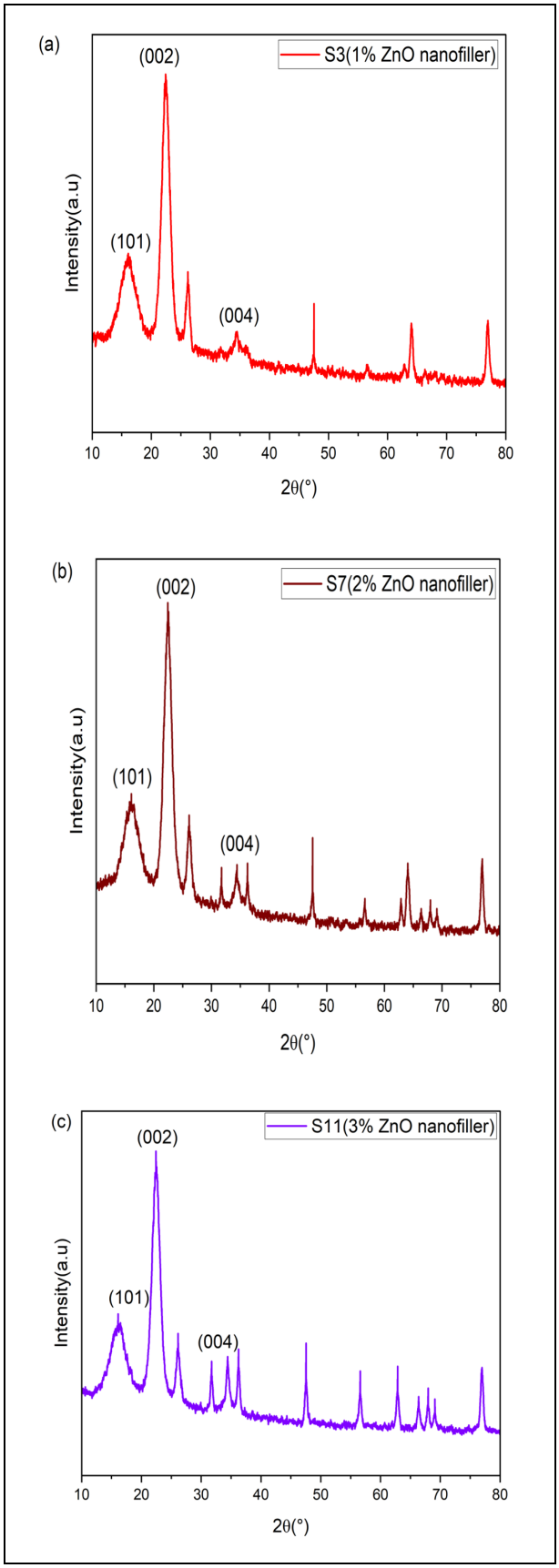

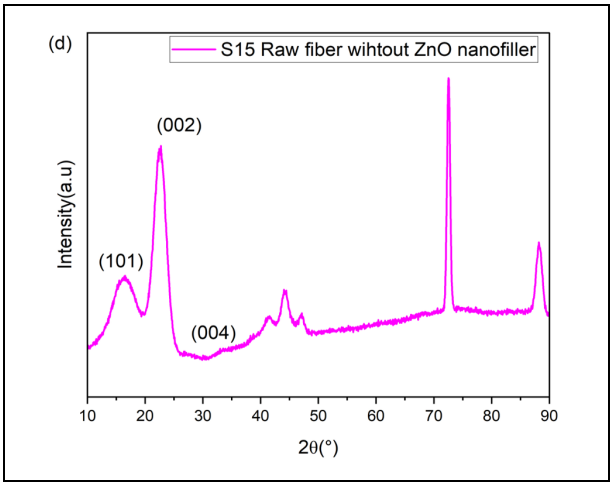

Fig. 7: XRD analysis of *Passiflora foetida* fibre with ZnO nanofiller composite (a) S3, (b) S7, (c) S11 and (d) S15

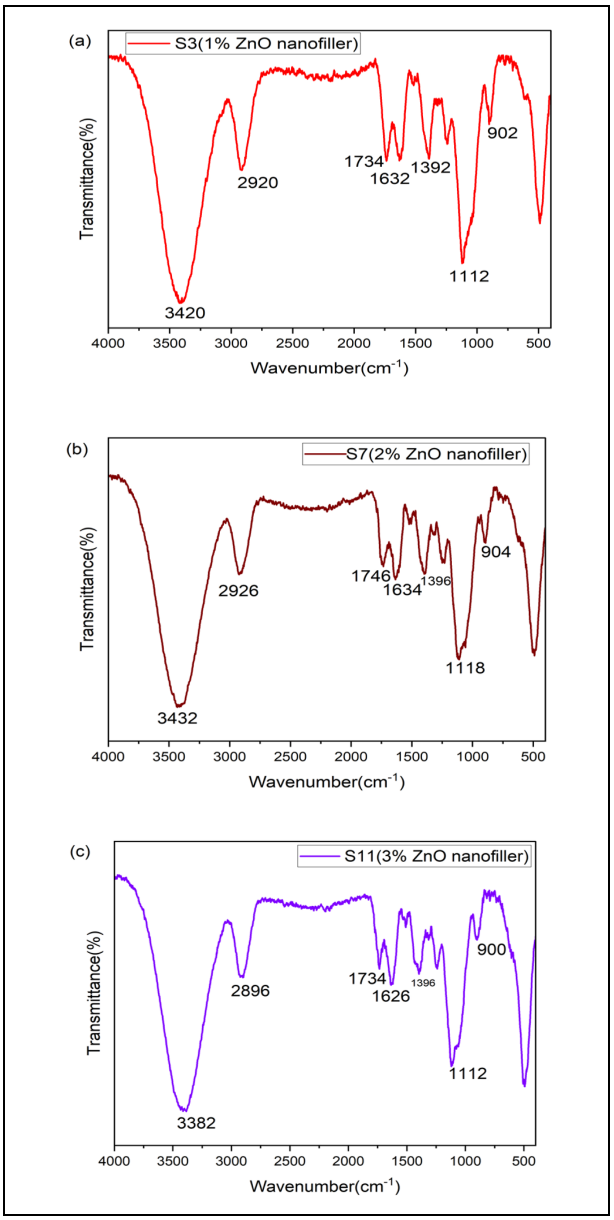

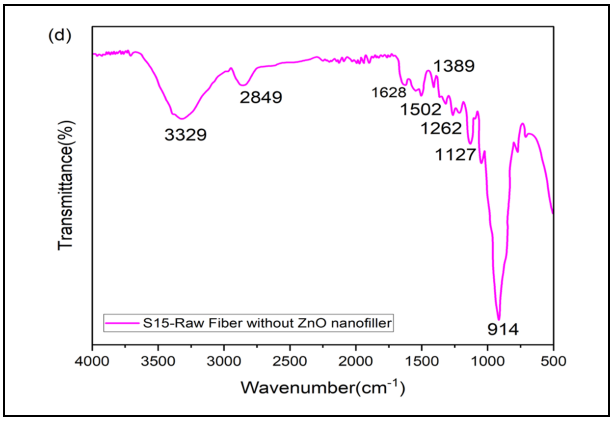

Fig. 8: FTIR analysis of *Passiflora foetida* fibre with ZnO nanofiller composite (a) S3, (b) S7, (c) S11 and (d) S15

FTIR was performed to find the functional groups in the *Passiflora foetida* fibers, ZnO nanofillers, epoxy matrix, and the fabricated composites, as well as to examine the chemical interactions among the constituent materials. The FTIR spectra exhibited characteristic absorption bands associated with the hydroxyl (O–H) stretching band in the limits of 3420–3432cm^{-1}, validating the occurrence of cellulose-rich functional groups in the natural fibers (Fig. 8a). Following alkali treatment, the reduction in the intensity of the carbonyl (C=O) absorption band near 1734-1746 cm^{-1} indicated the partial removal of hemicellulose and other amorphous constituents from the fiber surface. The absorption bands observed at 2920- 2926 cm^{-1} and 1112-1118 cm^{-1}, corresponding to C–H stretching and C–O–C stretching peaks, respectively, confirmed the presence of epoxy and cellulose structures within the composites (Figs. 8a and 8b).

A minor variation of the O–H absorption peak toward less transmission value was observed after the incorporation of ZnO nanofillers (Fig. 8c). This shift suggests the creation of stronger hydrogen-bonding interactions among the fiber, ZnO nanofiller, and epoxy matrix, leading to enhanced interfacial adhesion. The improved chemical compatibility among the constituents supports the enhanced mechanical properties obtained for the optimized composite formulation.

As shown in Fig. 8d, no additional absorption bands were detected in the composite spectra, indicating that the incorporation of ZnO nanofillers did not introduce new chemical bonds or alter the epoxy curing process. Instead, the observed interactions are predominantly physical in nature, arising from hydrogen bonding among the *Passiflora foetida* fibers, ZnO nanofillers, and epoxy matrix. Among the investigated composites, the composite consisting of 2 vol.% ZnO nanofiller showed the most effective interfacial adhesion between the reinforcing fibers and matrix. The enhanced molecular interactions identified from the FTIR spectra provide evidence of enhanced fiber–matrix adhesion.

The interfacial bonding observed is reflected in the superior mechanical performance of the optimized composite. In previous studies, FTIR analysis confirmed the presence of bioactive functional groups from *Passiflora foetida* fruit extract that acted as natural reducing, capping, and stabilizing agents during the green synthesis of AgNPs. These functional groups contributed to nanoparticle stabilization and successful surface functionalization, which was further supported by GC–MS analysis (Elangovan *et al.* 2022).

SEM was employed to analyze the morphological features of the fabricated composites to establish the relationship between their microstructural characteristics and mechanical performance (Fig. 9). The morphological surface of the sample without ZnO nanofiller exhibited extensive fiber pull-out, interfacial voids, and poor reinforcement–matrix contact, indicating inadequate interfacial adhesion. The incorporation of 1 vol.% ZnO nanofiller resulted in improved fiber embedding and a noticeable reduction in void formation, although some interfacial defects were still evident.

The S3 composite (Fig. 9a) exhibited moderate fiber–matrix adhesion with localized voids and partial interfacial debonding, indicating incomplete stress transfer. The S7 composite (Fig. 9b) showed the most compact fracture surface, with well-embedded fibers, strong fiber–matrix interfacial bonding, and minimal defects, confirming efficient nanoparticle dispersion and improved load transfer. In contrast, the S11 composite (Fig. 9c) revealed interfacial debonding, fiber pull-out cavities, and matrix cracking caused by ZnO nanoparticle agglomeration, which acted as stress concentration sites. The S15 composite (Fig. 9d), without ZnO reinforcement, exhibited extensive fiber pull-out and poor fiber–matrix adhesion, resulting in weak interfacial bonding and premature fracture. Overall, the SEM observations demonstrate that the incorporation of 2 vol.% green-synthesized ZnO nanoparticles (S7) produced the most homogeneous microstructure and strongest interfacial adhesion, which is consistent with the superior mechanical performance of the composite. Previous studies reported that SEM–EDX analysis revealed predominantly spherical silver nanoparticles with a uniform elemental distribution under optimized green synthesis conditions. The homogeneous morphology and effective dispersion confirmed the role of *Passiflora foetida* extract in producing stable and well-dispersed nanoparticles for biomedical applications (Handayani *et al.* 2026).

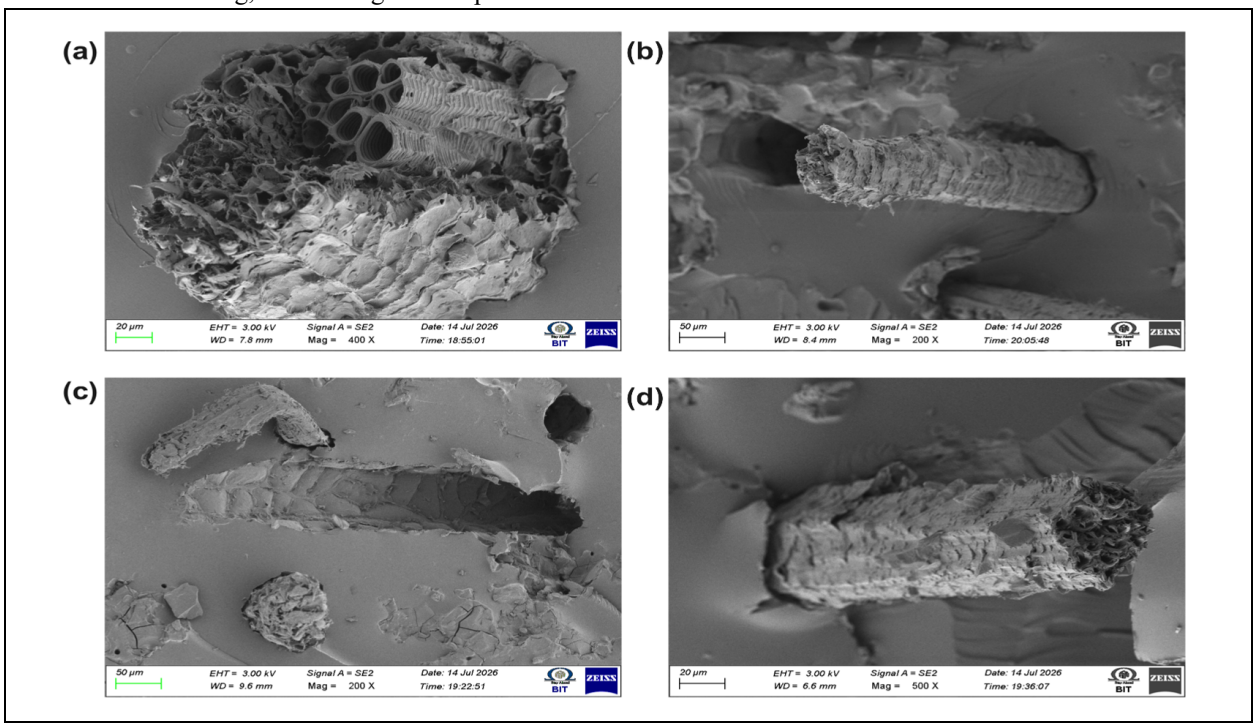

Fig. 9: SEM analysis of *Passiflora foetida* fibre with ZnO nanofiller composite (a) S3, (b) S7, (c) S11 and (d) S15

3.3 Physical Properties of the Composites

The physical performance of the composites was assessed through density, water absorption, and thickness swelling measurements to examine the influence of 30 vol.% *Passiflora foetida* fiber reinforced with 0, 1, 2, and 3 vol.% ZnO nanoparticles. The optimum fiber content (30 vol.%) was selected to eliminate the influence of fiber loading and evaluate only the contribution of ZnO nanoparticles. The S15 composite (0 vol.% ZnO) exhibited a density of 1.19 ± 0.01 g cm^{-3}, water absorption of 8.64 ± 0.28%, and thickness swelling of 7.83 ± 0.24% after 24 h immersion. The incorporation of 1 vol.% ZnO nanoparticles (S3)

increased the density to 1.22 ± 0.02 g cm^{-3}, while reducing the water absorption and thickness swelling to 7.18 ± 0.25% and 6.42 ± 0.21%, respectively. Among all the composites, the S7 composite (2 vol.% ZnO) exhibited the highest density (1.25 ± 0.01 g cm^{-3}) together with the lowest water absorption (5.94 ± 0.18%) and lowest thickness swelling (5.21 ± 0.17%), indicating excellent nanoparticle dispersion and strong fiber–matrix interfacial adhesion that effectively restricted moisture diffusion. However, increasing the ZnO content to 3 vol.% (S11) resulted in a slight reduction in density to 1.23 ± 0.01 g cm^{-3}, while the water absorption and thickness swelling increased to 6.71 ± 0.22% and 5.98 ± 0.20%, respectively. This deterioration is attributed to nanoparticle agglomeration, which created localized microvoids and facilitated water ingress.

3.4 Thermogravimetric Analysis

TGA was conducted on the composites containing 30 vol.% *Passiflora foetida* fiber reinforced with 1, 2, 3 and 0 vol.% green-synthesized guava leaf-derived ZnO nanoparticles, designated as S3, S7, S11, and S15, respectively (Fig. 10). The optimum fiber content (30 vol.%) was selected to analyze the impact of ZnO nanoparticle concentration on the thermal stability while eliminating the influence of fiber loading. All composites exhibited a typical three-stage thermal degradation profile. The initial weight loss below 90- 110 °C was due to the desorption of absorbed humidity and residual volatile constituents. The second decomposition stage, occurring between 300 and 390 °C, corresponded to the degradation of cellulose and hemicellulose present in the *Passiflora foetida* fibers. The final degradation stage above 510-700 °C was associated with lignin decomposition and degradation of the epoxy matrix, resulting in the creation of a steady carbonaceous residue.

Among the investigated composites, the S7 composite (30 vol.% fiber + 2 vol.% ZnO nanoparticles) exhibited the highest onset degradation temperature and the greatest residual char yield, indicating superior thermal stability. The improved thermal behavior is attributed to the homogeneous dispersion of ZnO nanoparticles, which acted as a thermal barrier and delayed heat transfer during degradation. In contrast, the S11 composite (3 vol.% ZnO) showed a slight reduction in thermal stability due to nanoparticle agglomeration, whereas the S15 composite (without ZnO) exhibited the lowest thermal resistance because of the absence of the protective nanofiller. These observations are consistent with the mechanical characterization, confirming that 2 vol.% ZnO nanoparticles provide the optimum reinforcement by improving both the thermal stability and fiber–matrix interfacial adhesion of the composite.

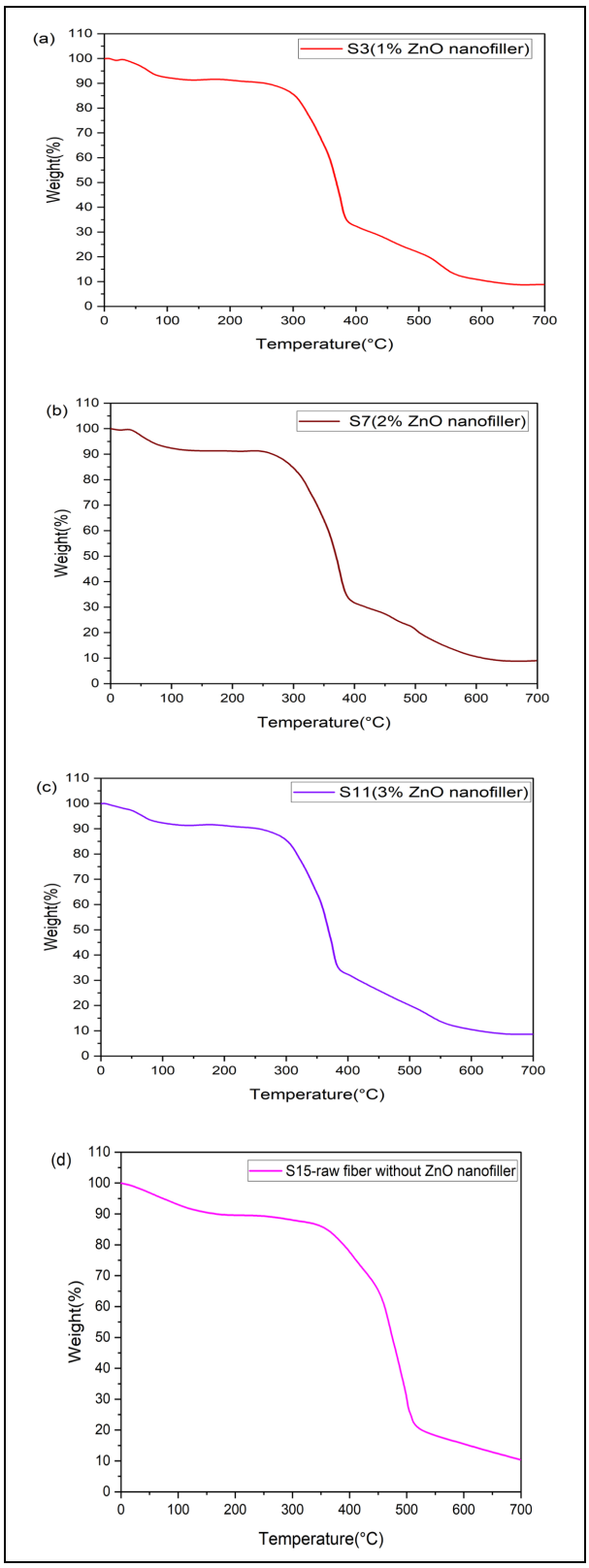

Fig. 10: TGA analysis of *Passiflora foetida* fibre with ZnO nanofiller composite (a) S3, (b) S7, (c) S11 and (d) S15

3.5 Antibacterial Activity of the Optimum Composites

The antibacterial activities of the optimum *Passiflora foetida* fiber/2 vol.% green-synthesized guava leaf-derived ZnO nanoparticle-reinforced epoxy composite (S7) were evaluated against different microorganisms through the agar disc diffusion technique. The inhibition zones are presented in Fig. 11.

The maximum inhibition zone of 22.8 ± 0.7 mm was noted for S. aureus, secondly 20.9 ± 0.6 mm for *B. subtilis*. Comparatively lower inhibition of 18.6 ± 0.5 mm and 16.9 ± 0.5 mm were recorded against *E. coli* and *P. aeruginosa*, respectively. The stronger antibacterial suspension against Gram (+) bacteria is attributed to their relatively simple cell wall structure, which allows easier penetration of Zn^{2+} ions and reactive oxygen species (ROS). In contrast, the outer lipopolysaccharide membrane of Gram (-) bacteria acts as an extra barrier, reducing susceptibility to ZnO nanoparticles.

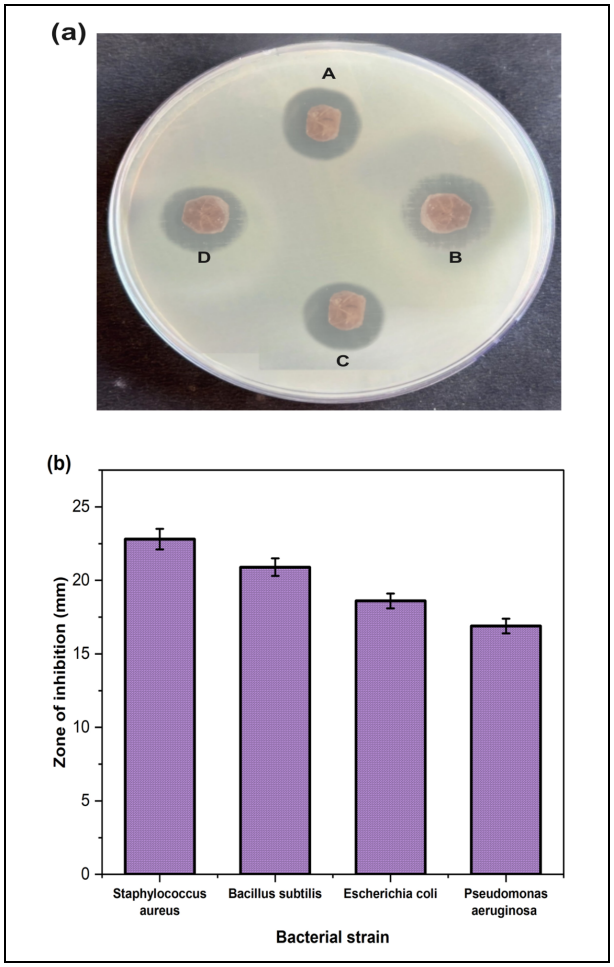

Fig. 11: Antibacterial activity of the optimum 30 vol% *Passiflora foetida* fiber/2 vol.% guava leaf-derived ZnO nanoparticle reinforced epoxy composite

The excellent antibacterial performance of the optimum composite is due to the homogeneous dispersion of 2 vol.% ZnO nanoparticles within the matrix, as evidenced by the superior interfacial bonding and homogeneous microstructure observed in the SEM analysis of the optimum composite. The ZnO nanoparticles continuously released Zn^{2+} ions and generated reactive oxygen species, including superoxide anion ions and hydroxyl radicals, which induced oxidative stress, disturbed bacterial cell membranes, and inhibited cellular metabolism, ultimately resulting in bacterial cell death. Furthermore, residual phytochemicals originating from the guava leaf extract may have enhanced the stability and surface activity of the ZnO nanoparticles, contributing to the observed antimicrobial performance. Previous studies have demonstrated that ZnO nanoparticle-treated cotton fabrics show strong antibacterial activity against airborne microorganisms and the Gram (-) bacterium *Pseudomonas aeruginosa* (Asaulyuk *et al.* 2024).

4. CONCLUSION

This study developed epoxy composites reinforced with *Passiflora foetida* fibers and guava-leaf-mediated ZnO nanoparticles**.** Among the evaluated formulations, S7, containing 30 vol.% fiber and 2 vol.% ZnO, exhibited the highest tensile strength (41.25 MPa), flexural strength (75.4 MPa), absorbed Izod impact energy (2.78 J), and hardness (94.3 Shore D). Increasing the ZnO content to 3 vol.% reduced mechanical performance, consistent with the greater occurrence of visible agglomerates and interfacial defects in SEM images. S7 exhibited a density of 1.25 ± 0.01 g cm^{-3}, water absorption of 5.94 ± 0.18%, and thickness swelling of 5.21 ± 0.17% after 24 h immersion. TGA showed multistage degradation involving initial moisture loss, major cellulose, hemicellulose, and epoxy decomposition between approximately 300 and 390 °C, followed by slower lignin degradation and char formation at higher temperatures. The S7 composite produced inhibition zones of 22.8 ± 0.7 mm against *S. aureus*, 20.9 ± 0.6 mm against *B. subtilis*, 18.6 ± 0.5 mm against *E. coli*, and 16.9 ± 0.5 mm against *P. aeruginosa*. These findings demonstrate measurable antibacterial activity under the tested conditions but do not establish quantitative bactericidal performance. The study was limited to short-term laboratory evaluation. Long-term durability, fatigue, creep, flame retardancy, UV stability, weathering, thermal cycling, biodegradation, toxicity, nanoparticle migration, and quantitative antibacterial performance require further investigation before packaging, automotive, structural, or hygienic applications can be proposed.

FUNDING

This research received no specific grant from any funding agency in the public, commercial, or not-for-profit sectors.

CONFLICTS OF INTEREST

The authors declare that there is no conflict of interest.

COPYRIGHT

This article is an open-access article distributed under the terms and conditions of the Creative Commons Attribution (CC BY) license (http://creativecommons.org/licenses/by/4.0/).

REFERENCES

Abd, K. N. H., Khor, P. S., Mohammad, M., Alam, M. and Alotaibi, R., Biogenic ZnO nanoclusters from *Passiflora foetida* extract: Synthesis, structural characterization, and MCF-7 cytotoxicity with DNA binding analysis, *J. Mol. Struct.*, 1371, 146400 (2026). https://doi.org/10.1016/j.molstruc.2026.146400

Ali, M. F., Hossain, M. S., Lithi, I. J., Ahmed, S. and Chowdhury, A. M. S., Fabrication and characterization of sustainable composites from animal fibers reinforced unsaturated polyester resin, *Heliyon*, 10(13), e33441 (2024). https://doi.org/10.1016/j.heliyon.2024.e33441

Armynah, B., Anugrahwidya, R. and Tahir, D., Composite cassava starch/chitosan/Pineapple Leaf Fiber (PALF)/Zinc Oxide (ZnO): Bioplastics with high mechanical properties and faster degradation in soil and seawater, *Int. J. Bio. Macromol.*, 213, 814–823 (2022). https://doi.org/10.1016/j.ijbiomac.2022.06.038

Asaulyuk, T., Semeshko, O., Saribyekova, Y., Kulish, I. and Horokhov, I., Effect of ZnO Nanoparticles Synthesized by the Improved Method on the Antibacterial Properties of Cotton Textile Materials, *Eastern-Europe. J. Enterprise Technol.*, 1(12(127)), 27–34 (2024). https://doi.org/10.15587/1729-4061.2024.297066

Barve, S. P., Sivasundar, V., Swapna Sri, M. N., Satishkumar, P., Raja, N. D., Krishnaraj, C., Haldar, B. and Mayakannan, S., Enhanced Mechanical and Tribological Performance of Casuarina Fiber-reinforced Epoxy Composites Using ZnO and ZrO_2 Nanoparticles, *J. Environ. Nanotechnol.*, 14(3), 705–714 (2025). https://doi.org/10.13074/jent.2025.09.2531750

Demir, M. E., The effect of filler type (tungsten carbide, zinc oxide) and content on the mechanical and wear behavior of jute/flax reinforced epoxy hybrid composites: Experimental and artificial neural network analysis, *Polym. Compos.*, 46(9), 8700–8719(2025). https://doi.org/10.1002/pc.29879

Edlabadkar, A. P., Chaudhari, S., Harak, S. S., Vijayakumar, M., Nanthakumar, S. and Mayakannan, S., Optimising Tensile and Impact Strength of Polyethylene-based Nanocomposites with Graphene, Carbon and Hemp Fibers, *Int. J. Veh. Struct. Syst.*, 18(1), 39–46 (2026). https://doi.org/10.4273/ijvss.18.1.08

Elangovan, D., Rahman, H. B. H., Dhandapani, R., Palanivel, V., Thangavelu, S., Paramasivam, R. and Muthupandian, S., Coating of wallpaper with green synthesized silver nanoparticles from *Passiflora foetida* fruit and its illustrated antifungal mechanism, *Process Biochem.*, 112, 177–182 (2022). https://doi.org/10.1016/j.procbio.2021.11.027

Fang, X., Xie, Y., Li, R. and Xu, W., Ferroconcrete-inspired synergistic modification of bamboo fiber/PLA biocomposites with enhanced interfacial compatibility and antibacterial performance, *Polym.*, 356, 130089 (2026). https://doi.org/10.1016/j.polymer.2026.130089

Ganesh, B. L., Sureshkumar, V., Pradeep, G. M., Tamilselvi, S., Shalom, N. and Girimurugan, R., Mechanical, moisture, and morphological evaluation of ZnO-modified vetiver root fiber epoxy bio composites for sustainable applications, *Interact.*, 247(1), 117 (2026). https://doi.org/10.1007/s10751-026-02491-0

Gupta, R. K., Saravanan, V., Manikandan, K., Shalom, N., Arun, K. K. and Mayakannan, S., Fatigue, impact, and mechanical behavior of tamarind cellulose reinforced birch/Khusha grass fiber hybrid bio composites, *Interact.*, 247(1), 104 (2026). https://doi.org/10.1007/s10751-026-02445-6

Handayani, S., Azmi, A. A., Rudiyanto, R., Ismail, W. I. W., Tarman, K., Abas, F., Khairul, W. M. and Maulidiani, M., Optimisation of Silver Nanoparticle Synthesis Using Aqueous Extract of *Passiflora foetida* L. via Response Surface Methodology, *Pertanika J. Sci. Technol.*, 34(2), 787–822 (2026). https://doi.org/10.47836/pjst.34.2.09

Harish, M. N., Bobby, J. S., Kuppusamy, P. G. and Annapoorani, C. L., Development and characterization of hybrid Kender-F fibre and collagen toughened epoxy composites, *Chem. Pap.*, (2026). https://doi.org/10.1007/s11696-026-05091-y

Koshy, J. T. and Sangeetha, D., Nanocellulose reinforced sustainable polyvinyl alcohol and pectin based nanocomposite films embedded with AgO/ZnO nano structures for wound dressing applications, *Sci. Rep.*, 16(1), 8343(2026). https://doi.org/10.1038/s41598-025-34411-7

Loganathan, S., Selvam, K., Govindasamy, M. and Habila, M. A., Bioynthesis and characterization of zinc oxide nanoparticles (ZnO-NPs) using *Passiflora foetida* Linn leaves extract and their biological applications, *Biomass Convers. Biorefine.*, 15(4), 5861–5871(2025). https://doi.org/10.1007/s13399-024-05593-3

Meravi, M. K. and Panchore, V., Tribological and mechanical characteristics of glass/flax fiber-ZnO reinforced epoxy hybrid composite, *Colloid Polym. Sci.*, 303(3), 411–426 (2025). https://doi.org/10.1007/s00396-024-05356-6

Muniyasamy, M. K., Kumar, M. D., Mohanram, B. B. K., Ramesh, K., Muraliraja, R. and Selvarani, A. G., Influence of Zinc Oxide Nanoparticles on the Properties of Banyan Fiber/Epoxy Composites for Biomedical Applications, *J. Environ. Nanotechnol.*, 14(3), 150–162 (2025). https://doi.org/10.13074/jent.2025.09.2521568

Ning, L. Y., Azmi, A. A. A. R., Ismail, W. I. W., Tarman, K., Abas, F. and Maulidiani, M., Antioxidant Properties and Chemical Profile of *Passiflora foetida* Extracts Determined by ATR-FTIR Metabolomics, *Malaysia. J. Chem.*, 25(3), 463–473 (2023). https://doi.org/10.55373/MJCHEM.V25I3.463

Popescu, M. C., Ungureanu, C., Buse, E., Nastase, F., Tucureanu, V., Suchea, M., Draga, S. and Popescu, M. A., Antibacterial efficiency of cellulose-based fibers covered with ZnO and Al_2O_3 by Atomic Layer Deposition, *Appl. Surf. Sci.*, 481, 1287–1298 (2019). https://doi.org/10.1016/j.apsusc.2019.03.268

Raja, T., Devarajan, Y., PS, R. R., Tiwari, A., Dash, S., Sellamuthu, P., Shukla, K. K. and Mehar, K., Fabrication and Characterization of ZnO-Enhanced Kevlar Fiber/Epoxy Composites for Advanced Lightweight Structural and Engineering Applications, *J. Nat. Fib.*, 23(1), 2635687(2026). https://doi.org/10.1080/15440478.2026.2635687

Sakti, A. M., Darmadi, D. B., Gapsari, F., Widodo, T. D. and Ganda, A. N. F., Enhancing the structural and antibacterial properties of soybean hull fibers via alkali treatment and zinc oxide nanocoating, *Clean. Waste Syst.*, 11, 100289 (2025). https://doi.org/10.1016/j.clwas.2025.100289

Sathish, K. R., Vandhana Devi, V., Nivedhitha, D. M., Srish Satya, S., Visakan, S., Bharath Sharma, S. and Sathish Kumar, S. B., Effect of nanoparticles in natural fiber reinforced polymer composites, *Mater. Today: Proce.*, 122, 24-31 (2026). https://doi.org/10.1016/j.matpr.2023.04.130

Seenivasan, S., Sathya, V., Jegadeeswaran, M., Nanthini, B., Prabhu, T. and Johnson, K. S., Influence of Cordia dichotoma Fibers and Zinc Oxide Nanoparticles on the Mechanical and Thermal Behavior of Epoxy Hybrid Composites, *J. Environ. Nanotechnol.*, 14(3), 215–222(2025). https://doi.org/10.13074/jent.2025.09.2531655

Senniangiri, N., Gokulkannan, S., Kumar, S. D. and Gokul, S., Enhancing Mechanical, Moisture Resistance, and Fire-retardant Properties of Nelumbo nucifera Fiber/Epoxy Nanocomposites with Zinc Oxide Nanoparticles, *J. Environ. Nanotechnol.*, 14(1), 253–265 (2025). https://doi.org/10.13074/jent.2025.03.2511215

Soshi, S. S., Tanvir, N. S., Khan, M. Y., Haque, M. R., Gafur, M. A., Islam, M. S. and Hasan, M., Characterisation of ZnO-doped novel woodnut fibre-reinforced hybrid polyester composite, *Adv. Mater. Proce. Technol.*, 1-21 (2026). https://doi.org/10.1080/2374068X.2026.2676578

Subbarao, E., Sharma, D., Singh, P., Gupta, R. K., Gayathri, B. and Mayakannan, S., Influence of B_4C and TiO_2 fillers on mechanical and tribological performance of Canna *indica/Curaua* fiber reinforced hybrid composites with ANN prediction, *Interact.*, 247(1), 148 (2026). https://doi.org/10.1007/s10751-026-02511-z

Tasnim, T., Rabbi, M. S., Adil, M. M. and Hasib, M. A., An experimental study on jute/banana fiber reinforced poly (vinyl alcohol) composites with nanofiller, *J. Vinyl Additive Technol.*, 30(5), 1327–1340 (2024). https://doi.org/10.1002/vnl.22127

Tumusiime, G., Wambua, P., Rwahwire, S., Njuguna, D. and Yiga, V. A., Production and mechanical characterization of reinforced zinc oxide nanoparticle-coated silk waste bio-composites, *Polym. Bull.*, 80(8), 8799–8818 (2023). https://doi.org/10.1007/s00289-022-04475-w

Yang, F., Nie, M. and Zhang, C., Interlocking interface design in epoxy resin composites via ZnO-functionalized cellulose for enhanced mechanical and multifunctional performance, *Colloids Surf. A: Physicochem. Eng. Aspects*, 749, 141399 (2026). https://doi.org/10.1016/j.colsurfa.2026.141399